A general approach to break the concentration barrier in single-molecule imaging

Loveland, Anna B.; Habuchi, Satoshi; Walter, Johannes C.; Oijen, Antoine M. van

Published in:
Nature Methods

DOI:
10.1038/nmeth.2174

Publication date:
2012

A general approach to break the concentration barrier in single-molecule imaging

Anna B Loveland[1–3], Satoshi Habuchi[1,3], Johannes C Walter[1,4] & Antoine M van Oijen[1,3,4]

Single-molecule fluorescence imaging is often incompatible with physiological protein concentrations, as fluorescence background overwhelms an individual molecule's signal. We solve this problem with a new imaging approach called PhADE (PhotoActivation, Diffusion and Excitation). A protein of interest is fused to a photoactivatable protein (mKikGR) and introduced to its surface-immobilized substrate. After photoactivation of mKikGR near the surface, rapid diffusion of the unbound mKikGR fusion out of the detection volume eliminates background fluorescence, whereupon the bound molecules are imaged. We labeled the eukaryotic DNA replication protein flap endonuclease 1 with mKikGR and added it to replication-competent *Xenopus laevis* egg extracts. PhADE imaging of high concentrations of the fusion construct revealed its dynamics and micrometer-scale movements on individual, replicating DNA molecules. Because PhADE imaging is in principle compatible with any photoactivatable fluorophore, it should have broad applicability in revealing single-molecule dynamics and stoichiometry of macromolecular protein complexes at previously inaccessible fluorophore concentrations.

The imaging of individual, fluorescently labeled macromolecules and their interactions with substrates or binding partners reveals aspects of biochemical reactions that are inaccessible in ensemble experiments[1]. However, single-molecule fluorescence experiments are only possible when fewer than one fluorescent molecule is present per diffraction-limited detection volume, which corresponds to a maximum concentration of ~1 nM. Total internal reflection (TIR) fluorescence microscopy can be used to confine the illuminated volume to an ~100-nm thin layer at a glass-water interface. Nevertheless, the highest concentration of fluorescent molecules compatible with TIR fluorescence microscopy is ~10 nM, far less than the dissociation constant for many biochemical interactions[2]. The illuminated volume can be further reduced in the far field in technically demanding approaches such as 4Pi and stimulated emission depletion microscopy[3,4]. Alternatively, the sample volume itself may be drastically limited[5,6], but this strategy precludes visualizing micrometer-scale motions. In summary, a generally applicable method is lacking to allow single-molecule imaging of biological macromolecules at physiologically relevant concentrations.

Here we describe an imaging scheme called PhADE that increases the useful concentration range of single-molecule fluorescence imaging by at least two orders of magnitude and allows single-molecule visualization at physiological concentrations. We validated this method in a challenging environment for single-molecule studies, an undiluted cell-free extract of *X. laevis* eggs, to visualize individual DNA replication complexes. This approach revealed the micrometer-scale movement of replication forks, the pattern of replication initiation along DNA molecules and the dynamics of individual proteins at replisomes.

RESULTS

In PhADE, a protein of interest is fused to the photoconvertible protein mKikGR[7]. The fusion protein is introduced into a microfluidic flow cell containing a binding partner or substrate that has been immobilized on the surface (**Fig. 1a**). In its ground state, mKikGR fluoresces green (mKikG) upon excitation with 488-nm light (**Supplementary Fig. 1**). After illumination with a pulse of 405-nm light, the green form of the fluorophore is converted or 'activated' to a spectrally distinct form (mKikR) that fluoresces red upon excitation with 568-nm light (**Supplementary Fig. 1**). Using TIR microscopy, mKikG is selectively converted to mKikR near the surface of the flow cell (**Fig. 1a**). Any mKikR molecules not bound to the binding partner diffuse out of the TIR illumination volume and are diluted by diffusion-driven exchange with nonactivated protein. Finally, the mKikR molecules retained by the binding partner are imaged with 568-nm TIR excitation until they dissociate or photobleach.

To validate PhADE, a solution of 2 μM 6×His-tagged mKikGR was drawn into a flow cell coated with a low density of surface-immobilized anti-6×His antibody. As expected, TIR imaging of mKikG with 488-nm light resulted in saturated images, and imaging

[1]Department of Biological Chemistry and Molecular Pharmacology, Harvard Medical School, Boston, Massachusetts, USA. [2]Graduate Program in Biophysics, Harvard University, Cambridge, Massachusetts, USA. [3]Present addresses: Department of Biochemistry, Brandeis University, Waltham, Massachusetts, USA (A.B.L.), Division of Chemical and Life Sciences and Engineering, King Abdullah University of Science and Technology, Thuwal, Kingdom of Saudi Arabia (S.H.) and The Zernike Institute for Advanced Materials, University of Groningen, Groningen, The Netherlands (A.M.v.O.). [4]These authors contributed equally to this work. Correspondence should be addressed to J.C.W. (johannes_walter@hms.harvard.edu) or A.M.v.O. (a.m.van.oijen@rug.nl).

RECEIVED 19 APRIL; ACCEPTED 9 AUGUST; PUBLISHED ONLINE 9 SEPTEMBER 2012; DOI:10.1038/NMETH.2174

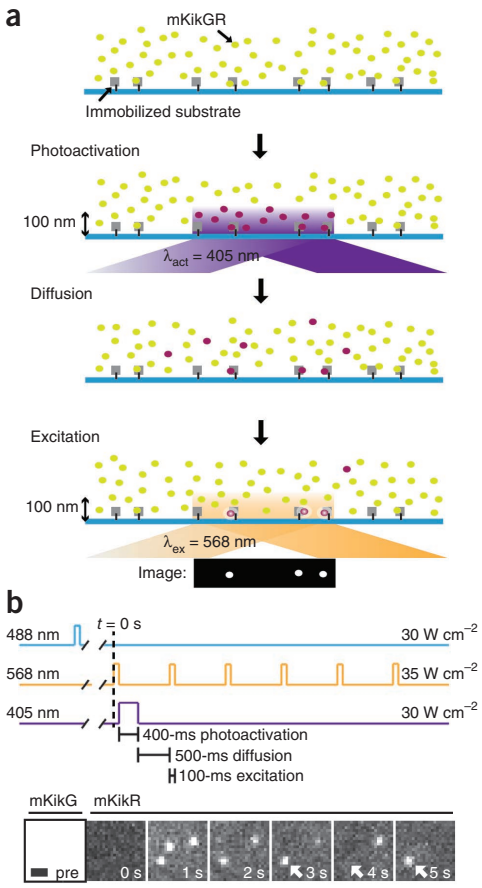

Figure 1 | Experimental design and validation of PhADE. (**a**) Cartoon depicting the three steps of the PhADE imaging scheme. (**b**) 6×His-mKikGR bound to anti-6×His antibody (substrate), which was immobilized on a surface via a biotin-streptavidin interaction, was imaged in the presence of 2 μM 6×His-mKikGR in solution. mKikG was imaged using 488-nm light ('pre'). Next, mKikR was imaged with 568-nm light before ('0 s') and after 405-nm photoactivation (panels '1 s' to '5 s') using the pulse sequence shown above. White arrows highlight an on-off intensity change indicative of a single mKikR molecule. Scale bar, 1 μm.

with 568-nm light before photoactivation failed to reveal any mKikR. However, after 405-nm activation of mKikG to mKikR and diffusion, discrete signals of mKikR were detected with a high signal-to-background ratio. The quantized on-and-off intensity changes confirm that signals correspond to single molecules (**Fig. 1b**). The photophysical properties of mKikGR allow a highly efficient conversion of immobilized mKikG to mKikR under our illumination conditions, and the majority of mKikGR can be photoconverted (**Supplementary Fig. 2**). Thus, PhADE can efficiently detect individual proteins bound to substrate in a highly concentrated solution of the labeled protein of interest.

We next wanted to apply PhADE to study a complex biochemical reaction. We chose eukaryotic DNA replication, which begins at thousands of chromosomal sites called origins[8]. In the G1 phase of the cell cycle, pre-replication complexes (pre-RCs) are assembled at origins. In the S phase, cyclin-dependent kinase (CDK) converts pre-RCs into pairs of replisomes that copy DNA in opposite directions, giving rise to replication 'bubbles' that consist of two double-stranded daughter DNA molecules. Unlike the leading strand, which is synthesized continuously, the lagging strand is made discontinuously from short, RNA-primed DNA segments called Okazaki fragments[9]. When the polymerase at the growing 3′ end of one Okazaki fragment encounters the 5′ end of another Okazaki fragment, it performs strand-displacement synthesis, creating a 5′ flap containing the primer. The processivity factor proliferating cell nuclear antigen (PCNA) then helps recruit a flap endonuclease (Fen1) that cleaves the flap. Several rounds of displacement synthesis and flap cleavage leave a ligatable nick[9]. Using DNA-fiber techniques[10], researchers have visualized eukaryotic DNA replication intermediates on individual strands of DNA, but no dynamic, single-molecule imaging of this process has been reported.

Eukaryotic DNA replication occurs with high efficiency in soluble, cell-free extracts of *X. laevis* eggs[11]. Performing conventional single-molecule imaging in such a system is challenging because fluorescent proteins would have to be added at high concentrations to effectively compete with their endogenous counterparts, which are very abundant (100 nM–5 μM; **Supplementary Fig. 3a**; ref. 12). We reasoned that PhADE might overcome this problem because it allows single-molecule imaging at high fluorophore concentrations.

To apply PhADE to eukaryotic DNA replication, λ DNA (48.5 kb, contour length 16.3 μm) was stretched to ~80% of its contour length and attached at both ends to the bottom surface of a microfluidic flow cell (**Fig. 2a**). Next, a high-speed supernatant (HSS) of crude *X. laevis* egg lysate was introduced that assembles pre-RCs in a sequence-nonspecific manner[13]. After 20 min, HSS was replaced with nucleoplasmic extract (NPE), which promotes DNA replication[11,14] (**Fig. 2a**). The immobilized DNA replicates efficiently, and multiple replication bubbles can be visualized via immunofluorescent detection of incorporated digoxigenin-dUTP or labeling of dsDNA with an intercalating dye (SYTOX Orange) whose fluorescence intensity doubles at replicated regions[15] (**Fig. 2a**). To implement PhADE, we prepared a fusion of Fen1 with mKikGR (**Supplementary Fig. 3b**) and confirmed that it interacted specifically with PCNA[16] (**Supplementary Fig. 3c**), cleaved 5′ flap DNA[17,18] (**Supplementary Fig. 3d**) and, like endogenous Fen1, was able to function in the maturation of Okazaki fragments into a continuous lagging strand (**Supplementary Fig. 3e–i**, **Supplementary Methods**).

For PhADE imaging of replication in the flow cell, NPE was supplemented with 2–4 μM Fen1^{KikGR}. For most experiments, we used a nuclease-deficient mutant of Fen1^{KikGR} (D179A Fen1^{KikGR}; **Supplementary Fig. 3d**) to minimize the potential for nucleolytic damage to the tethered DNA. At a concentration of 2–4 μM, D179A Fen1^{KikGR} should compete with endogenous Fen1, which is present in the replication reaction at ~1 μM (**Supplementary Fig. 3a**). For the initial PhADE experiments, origin firing was restricted to about one event per λ phage to prevent merging of neighboring replication bubbles[11,15] (**Supplementary Fig. 4a**,**b**). Once replication began, we performed cycles of PhADE imaging at 10-s intervals (**Fig. 2b**). A kymograph of the images revealed a growing, linear tract of D179A Fen1^{KikR} that coincided with replicated DNA (**Fig. 2c** and **Supplementary Video 1**). The high intensity of the signals at an excitation power tenfold lower than necessary to image single molecules (**Fig. 1b**) suggests that many molecules of D179A Fen1^{KikGR} were bound along the length of each replication bubble. Nevertheless, PhADE imaging of Fen1^{KikR} greatly increased the contrast of features that

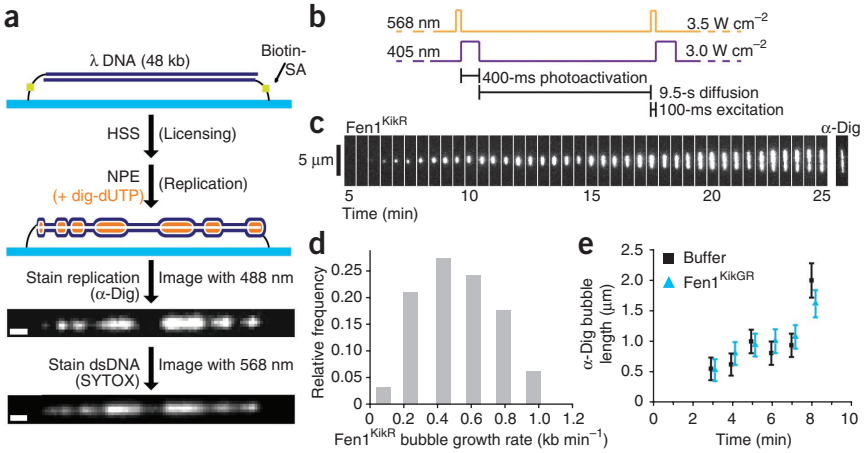

Figure 2 | PhADE imaging of Fen1^{KikR} visualizes the growth of individual replication bubbles. (**a**) Scheme for replication of surface-immobilized λ DNA by *X. laevis* egg extracts and detection of replication bubbles. λ DNA is attached to the bottom surface of a flow cell at both ends. Next, the DNA is licensed with high-speed supernatant (HSS). Replication is promoted with nucleoplasmic extract (NPE) supplemented with digoxigenin (dig)-dUTP and, for PhADE imaging, Fen1^{KikGR}. After real-time imaging of Fen1^{KikR} (see below), the extracts are removed, and replicated DNA is stained with anti–digoxigenin-fluorescein Fab fragments (α-Dig) and/or SYTOX Orange. Scale bars, 1 μm. (**b**) PhADE sequence used to visualize the growth of D179A Fen1^{KikR}–labeled replication bubbles. (**c**) Replication was carried out in the presence of 4 μM D179A Fen1^{KikGR} and dig-dUTP under conditions of limited origin firing (**Supplementary Fig. 4a**,**b**). Between 5 and 25 min after the first NPE addition, D179A Fen1^{KikR} was imaged every 10 s using PhADE. A sample kymograph shows every third frame of a replication bubble growing over time. After the last PhADE cycle, replicated DNA was stained with α-Dig. (**d**) Histogram of bubble growth rates tracked between 5 and 25 min displays a mean of 520 ± 220 bp min^{-1} (±s.d.; n = 62 events from three independent experiments). (**e**) Average length of replication bubbles as measured by α-Dig staining, in the presence (blue triangles) or absence (black squares) of 2 μM D179A Fen1^{KikGR}. Mean ± error estimate (Online Methods and **Supplementary Table 1**).

were barely distinguishable using TIR fluorescence imaging of Fen1^{KikG} (**Supplementary Fig. 4c**,**d**). The growth of 62 D179A Fen1^{KikR} bubbles imaged using the PhADE regime in **Figure 2b** was tracked, and a mean growth rate of 520 ± 220 (± s.d.) bp min^{-1} (**Fig. 2d**) was revealed, in agreement with previous estimates of the replication fork rate in egg extracts[15]. We verified that these PhADE imaging conditions supported the visualization of the replication reaction for at least 12 min without slowing growth (**Supplementary Fig. 4e**).

The binding of Fen1^{KikGR} along the entire length of replication bubbles was unexpected because Okazaki-fragment maturation is thought to occur only immediately behind the replication fork[9,19]. This phenomenon was explained by the fact that high concentrations of Fen1^{KikGR} induced the retention of PCNA on DNA, effectively creating a continuous tract of Fen1^{KikGR} docking sites (**Supplementary Fig. 4f**,**g**). Notably, because 2 μM D179A Fen1^{KikGR} does not detectably alter ensemble replication kinetics (**Supplementary Fig. 4h**) or single-molecule bubble growth (**Fig. 2e** and **Supplementary Table 1**), Fen1^{KikGR} PhADE is a valid means to visualize the dynamics of replication bubbles.

We next used D179A Fen1^{KikGR} PhADE to follow replication when origin firing was unrestricted. Starting 2.5 min after NPE addition, iterative PhADE cycles as depicted in **Figure 2b** revealed the global, time-resolved pattern of replication on individual λ DNAs (**Fig. 3a** and **Supplementary Video 2**). We verified that all replication bubbles were detected with PhADE (**Supplementary Fig. 5a**,**b**). On the basis of these PhADE movies, we quantified the timing and spacing of replication initiation events reported by Fen1^{KikR} signals that appear and increase in intensity and then in size (**Fig. 3a**; see Online Methods for criteria). Initiations detected by Fen1^{KikGR} peaked 6 min after addition of NPE (**Fig. 3b** and **Supplementary Fig. 5c**). Above the resolution limit of 0.5 μm, the distribution of interorigin distances was well fitted by an exponential decay (**Fig. 3c**), suggesting that origin spacing is random at these length scales. Notably, the cumulative interorigin distance measured by PhADE declined to 3.0 ± 1.0 kb (0.79 ± 0.27 μm) by

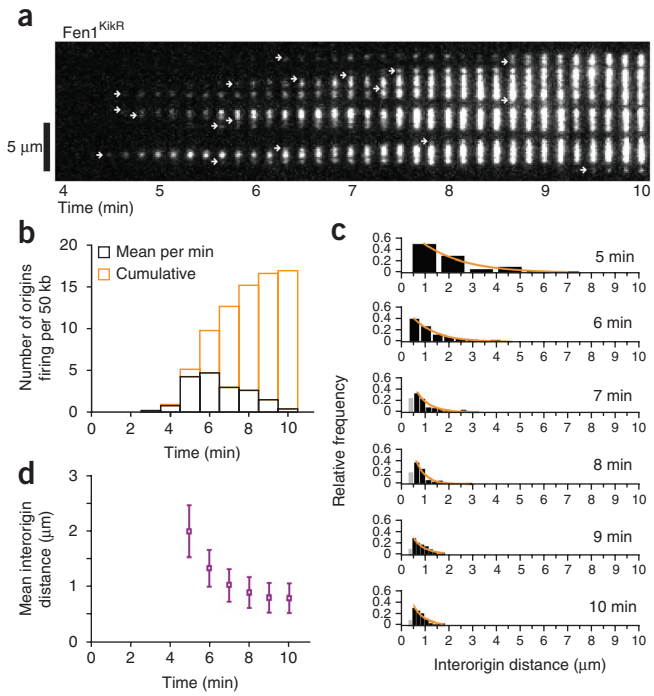

Figure 3 | During unperturbed replication, PhADE imaging of Fen1^{KikR} reveals a high density of initiations. (**a**) Replication of λ DNA during unrestricted origin firing was monitored by PhADE imaging (as in **Fig. 2b**) of 2 μM D179A Fen1^{KikGR} and displayed as a kymograph. White arrows indicate initiations. (**b**) PhADE kymographs as in **a** were analyzed to determine the mean number of origins firing each minute (black) or cumulatively (orange) per λ DNA (n = 12 λ DNA). Similar results were obtained in a second extract (**Supplementary Fig. 5c**). (**c**) PhADE kymographs as in **a** were analyzed to determine the distance between adjacent initiations over time. Black bars, reliable resolution limit (>0.5 μm); orange lines, single exponential decay fit to bars >0.5 μm. (**d**) The mean interorigin distance as determined from 12 replicating λ DNA molecules followed via D179A Fen1^{KikR} PhADE declines over time. Mean ± error estimate (Online Methods). Similar results were obtained in a second extract (**Supplementary Fig. 5d**).

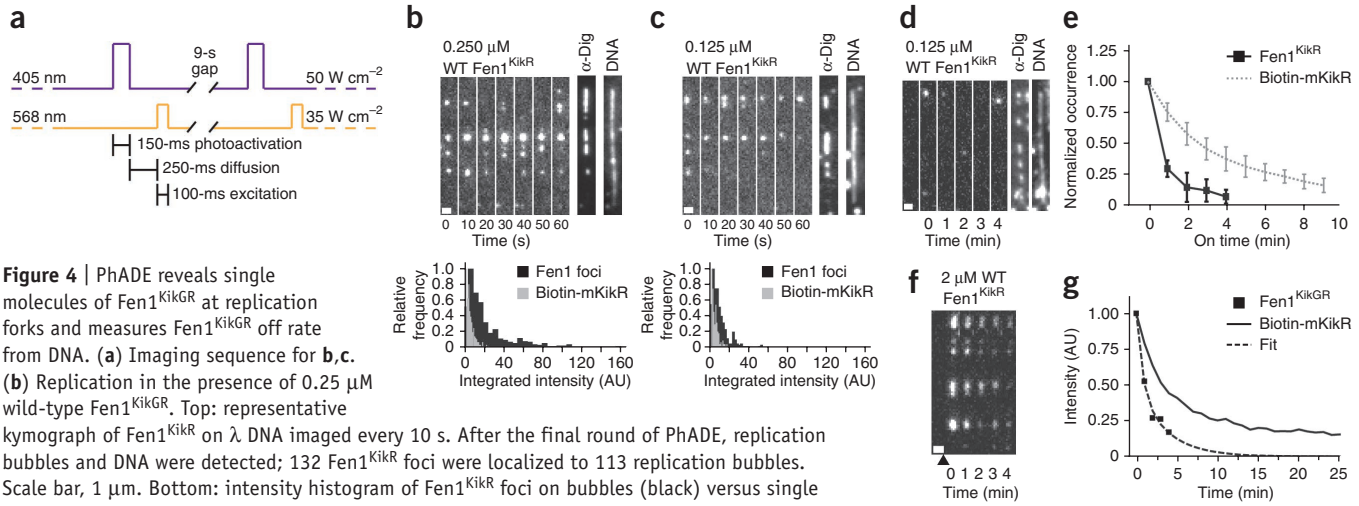

Figure 4 | PhADE reveals single molecules of Fen1^{KikGR} at replication forks and measures Fen1^{KikGR} off rate from DNA. (**a**) Imaging sequence for **b**,**c**. (**b**) Replication in the presence of 0.25 μM wild-type Fen1^{KikGR}. Top: representative kymograph of Fen1^{KikR} on λ DNA imaged every 10 s. After the final round of PhADE, replication bubbles and DNA were detected; 132 Fen1^{KikR} foci were localized to 113 replication bubbles. Scale bar, 1 μm. Bottom: intensity histogram of Fen1^{KikR} foci on bubbles (black) versus single molecules of biotin-mKikR (gray). AU, arbitrary units; α-Dig, anti–digoxigenin-fluorescein Fab fragments. (**c**) Replication as in **b**, but using 0.125 μM wild-type Fen1^{KikGR}; 112 Fen1^{KikR} foci were found on 129 replication bubbles. Scale bar, 1 μm. (**d**) DNA was replicated in the presence of 0.125 μM wild-type Fen1^{KikGR}, and Fen1^{KikR} was imaged as in **Supplementary Figure 7a** before (frame 1) and after (frames 2–6) photoactivation. Afterward, replication bubbles and DNA were detected. Scale bar, 1 μm. (**e**) The duration of wild-type Fen1^{KikR} binding at replication bubbles is compared to the fluorescence on times of immobilized biotin-mKikR (wild-type Fen1^{KikR}: mean ± s.d. of three experiments, n = 40 events; biotin-mKikR: mean ± s.d. of six experiments, n = 1,165 events, points are fit to a monoexponential decay). (**f**) DNA was replicated in the presence of 2 μM WT Fen1^{KikGR}. Fen1^{KikR} was photoactivated once (black triangle) and imaged once per minute as depicted in **Supplementary Figure 7c**. Scale bar, 1 μm. (**g**) Normalized, integrated intensity of the region in **f** (squares) is compared to biotin-mKikR photobleaching (solid line) under the same imaging conditions. Biexponential fit (dashed line) reveals a mean lifetime of 0.7 ± 0.3 min (± standard error of fit) for Fen1^{KikGR} on DNA.

10 min (**Fig. 3d** and **Supplementary Fig. 5d**), which is much less than values of 5–15 kb reported previously for plasmids or sperm chromatin replicating in *X. laevis* egg extracts[20–25]. The data in **Figures 2** and **3** demonstrate that PhADE can be used to monitor the movement of molecular machines over micrometer-scale distances at high fluorophore concentration.

We next wanted to know whether PhADE could detect single molecules of Fen1 at the DNA replication fork. We therefore supplemented replication reactions with 125 or 250 nM wild-type Fen1^{KikGR} and performed PhADE at higher illumination intensity (**Fig. 4a**). At these reduced concentrations, discrete foci of mKikR fluorescence were observed that colocalized with the ends of replication bubbles (**Fig. 4b**,**c**). A comparison of the fluorescence intensity of the foci to immobilized biotin-KikGR revealed that at 125 nM wild-type Fen1^{KikGR}, most foci correspond to single molecules (**Fig. 4c**). At 250 nM Fen1^{KikGR}, multiple molecules are found within foci (**Fig. 4b**). Notably, at concentrations of Fen1^{KikGR} that would be compatible with conventional TIR fluorescence imaging (10 nM; ref. 2), no signal was detected on the DNA, thereby demonstrating the need to perform PhADE under these conditions (**Supplementary Fig. 6a**). In contrast, ΔPIP Fen1^{KikGR}, which is deficient for PCNA-binding (**Supplementary Fig. 3c**), bound replication bubbles much less efficiently than wild-type Fen1^{KikGR} (**Supplementary Fig. 6b**). Thus, PhADE imaging is able to detect the specific binding of single Fen1^{KikR} molecules to the replisome, to estimate their stoichiometry, and to distinguish the properties of wild-type and mutant proteins.

To measure the dissociation rate of Fen1 from replication forks, Fen1^{KikGR} was photoactivated, and the number of frames that Fen1^{KikR} molecules persisted on DNA ('on time') when imaged once per minute was determined. To this end, we used iterative PhADE cycles to both efficiently activate new molecules and keep previously activated Fen1^{KikR} in the fluorescent state (**Supplementary Fig. 7a**,**b**). The on time of Fen1^{KikR} was clearly less than that of a biotin-mKikR standard immobilized through binding to streptavidin (**Fig. 4d**,**e**). The data suggest that the half-life of single molecules of Fen1^{KikR} at replication forks is less than 1 min. This time was similar to the half-life of Fen1^{KikR} on DNA at 2 μM Fen1^{KikGR}, which was 30–40 s (**Fig. 4f**,**g**). Thus, PhADE imaging can be used to measure not only the steady-state levels of proteins in a macromolecular complex but also their off rate from the complex.

DISCUSSION

PhADE represents a powerful means to achieve quantitative labeling and imaging of a fluorescent reactant with a high signal-to-noise ratio over a broad range of concentrations. The high-concentration regime will be useful for single-molecule studies of proteins with weak affinities for their targets and for cases in which a fluorescent protein must compete with its endogenous counterpart (**Supplementary Fig. 6a**). Factors that dissociate and reassociate rapidly can be imaged with repeated rounds of PhADE. Off rates can be determined with a single round of photoactivation followed by repeated imaging of the activated form. The arrival of new reactant to the substrate as a function of time elapsed between photoactivations will give access to on rates. PhADE imaging also allows the measurement of the number of fluorescently labeled proteins in a macromolecular complex over time. In principle, PhADE can be applied to the study of any biochemical reaction involving high reactant concentrations, provided that one reaction partner is immobilized on a surface.

Although mKikGR has excellent photoactivation properties, it is important to consider the suitability of mKikGR as a fluorescent tag for studying protein dynamics. We showed that Fen1^{KikGR} suppresses an apparent defect in Okazaki-fragment processing, which indicates that mKikGR does not adversely affect Fen1

function. However, at micromolar concentrations, Fen1^{KikGR} enhanced chromatin association of Fen1's binding partner PCNA. This effect allowed us to use Fen1 as a marker for replicated DNA. Notably, a high concentration of recombinant 6×His-tagged Fen1 did not stabilize PCNA (**Supplementary Fig. 4g**), thereby indicating that this effect was due to mKikGR. Because mKikGR is reported to be a monomer[7,26], and the off rates for Fen1^{KikR} at the high- and low-concentration regimes were similar (**Fig. 4**), we consider it unlikely that PCNA was stabilized owing to dimerization of Fen1^{KikGR} molecules bound to adjacent PCNA subunits. Instead, the bulkiness of the mKikGR tag might interfere with a protein-protein interaction important for PCNA dissociation. In short, mKikGR fusions can function normally, but whether subtle aspects of protein dynamics are affected can be difficult to ascertain, as is the case for all tagged proteins.

We used the distribution of Fen1^{KikR} fluorescence to measure the density of replication initiation events on a stretched chromosome. Even though a fraction of Fen1^{KikR} spots appeared not to grow, the observation that these foci exhibited a gradual increase in fluorescence, consistent with continual PCNA and Fen1 loading, suggests bona fide initiation and bubble formation, albeit at a length scale smaller than a diffraction-limited spot (<1.5 kb). Our data indicate that the spacing of all initiation events is two- to threefold higher than in previous static data sets[21–25,27]. This discrepancy is unlikely to be due to incomplete chromatinization of our doubly tethered DNA templates (**Supplementary Fig. 8** and **Supplementary Table 2**). Notably, a reanalysis of our dynamic data in a static fashion (by considering only individual frames from PhADE movies) resulted in a minimum center-to-center distance among replication bubbles that agrees with the previously published data (7.5 ± 1.0 kb; **Supplementary Fig. 5a**). The difference between the dynamic and static data sets is thus independent of the particular conditions under which replication is carried out. Rather, as previously anticipated[27], merging of replication bubbles and late-firing origins render more than 50% of initiations invisible to conventional DNA-combing approaches that analyze a single time point.

Our data also bear on the mechanism of Okazaki-fragment processing. If the 30- to 40-s on time of Fen1^{KikGR} accurately reflects the behavior of endogenous Fen1 (see above), the data are consistent with the proposal that a single Fen1 remains associated with PCNA and polymerase δ through multiple rounds of flap cleavage[28].

Together with recent work on RNA splicing, our experiments are among the first to use single-molecule fluorescence techniques to study macromolecular complexes in cell-free extracts[29,30]. Although immunodepletion of extracts (**Supplementary Fig. 3e–i**) and reconstitution with recombinant protein could be used to replace the endogenous Fen1 with Fen1^{KikGR}, this procedure is laborious, and we circumvented it through PhADE imaging of high concentrations of Fen1^{KikGR} added to undepleted extracts. In genetically tractable cell-free systems (such as yeast), the endogenous protein can be replaced by an mKikGR fusion or can be depleted via a genetically engineered degron tag. Whatever the particular approach, single-molecule studies in cell-free systems have the potential to yield novel biochemical insights into complex cellular pathways.

It should be possible to perform PhADE with a broad range of photoactivatable fluorophores. Ideally, PhADE probes should have high quantum yields and high extinction coefficients of photoactivation and fluorescence, as such properties speed up activation and minimize exposure of the sample to light. The probes must also have high switching yields to be compatible with use at high concentrations[31]. Optimizing photostability by decreasing photobleaching rates will aid single-molecule tracking. Finally, pairs of fluorophores that are switched by the same wavelength yet whose fluorescence spectra are distinct would allow for dual-color PhADE. Strong candidates for improved fluorophores are the azido-push-pull fluorogens[32] and Cy3-Cy5 heterodimers[33,34]. Single-molecule high-resolution fluorescence imaging techniques including photoactivated localization microscopy (PALM), fluorescence photoactivation localization microscopy (FPALM) and stochastic optical reconstruction microscopy (STORM) already rely on and are driving further innovations in photoswitchable fluorescent probes[35] that will likely be usable in PhADE.

METHODS

Methods and any associated references are available in the online version of the paper.

Note: Supplementary information is available in the online version of the paper.

ACKNOWLEDGMENTS

We thank H. Yardimci and J.J. Loparo for assistance with experiments and critical reading of the manuscript and C.G. Havens (Harvard University) for sharing advice and reagents. This work was supported by grants from the US National Institutes of Health (NIH) (GM077248), American Cancer Society (RSG0823401GMC) and Netherlands Organization for Scientific Research (NWO; Vici 680-47-607) to A.M.v.O. as well as by grants from the NIH (GM62267) and American Cancer Society (RSG0823401GMC) to J.C.W. A.B.L. was supported by the NIH and National Institute of General Medical Sciences Molecular Biophysics Training Grant (T32 GM008313).

AUTHOR CONTRIBUTIONS

A.B.L. performed all experiments. A.M.v.O. and S.H. designed the microscope. A.B.L., A.M.v.O. and J.C.W. designed experiments and performed data analysis. A.B.L., A.M.v.O. and J.C.W. prepared the manuscript.

COMPETING FINANCIAL INTERESTS

The authors declare no competing financial interests.

Published online at http://www.nature.com/doifinder/10.1038/nmeth.2174. Reprints and permissions information is available online at http://www.nature.com/reprints/index.html.

1. Joo, C., Balci, H., Ishitsuka, Y., Buranachai, C. & Ha, T. Advances in single-molecule fluorescence methods for molecular biology. *Annu. Rev. Biochem.* **77**, 51–76 (2008).
2. van Oijen, A.M. Single-molecule approaches to characterizing kinetics of biomolecular interactions. *Curr. Opin. Biotechnol.* **22**, 75–80 (2011).
3. Klar, T.A. & Hell, S.W. Subdiffraction resolution in far-field fluorescence microscopy. *Opt. Lett.* **24**, 954–956 (1999).
4. Hell, S. & Stelzer, E.H.K. Properties of a 4Pi confocal fluorescence microscope. *J. Opt. Soc. Am. A* **9**, 2159–2166 (1992).
5. Levene, M.J. *et al.* Zero-mode waveguides for single-molecule analysis at high concentrations. *Science* **299**, 682–686 (2003).
6. Boukobza, E., Sonnenfeld, A. & Haran, G. Immobilization in surface-tethered lipid vesicles as a new tool for single biomolecule spectroscopy. *J. Phys. Chem. B* **105**, 12165–12170 (2001).
7. Habuchi, S., Tsutsui, H., Kochaniak, A.B., Miyawaki, A. & van Oijen, A.M. mKikGR, a monomeric photoswitchable fluorescent protein. *PLoS ONE* **3**, e3944 (2008).
8. Masai, H., Matsumoto, S., You, Z., Yoshizawa-Sugata, N. & Oda, M. Eukaryotic chromosome DNA replication: Where, when, and how? *Annu. Rev. Biochem.* **79**, 89–130 (2010).
9. Burgers, P.M.J. Polymerase dynamics at the eukaryotic DNA replication fork. *J. Biol. Chem.* **284**, 4041–4045 (2009).

10. Herrick, J. & Bensimon, A. Introduction to molecular combing: genomics, DNA replication, and cancer. in *DNA Replication: Methods and Protocols* (eds. Vengrova, S. & Dalgaard, J.Z.) Ch. 5, 71–101 (Humana, Totowa, NJ, 2009).
11. Walter, J., Sun, L. & Newport, J. Regulated chromosomal DNA replication in the absence of a nucleus. *Mol. Cell* **1**, 519–529 (1998).
12. Strausfeld, U.P. *et al.* Cip1 blocks the initiation of DNA replication in *Xenopus* extracts by inhibition of cyclin-dependent kinases. *Curr. Biol.* **4**, 876–883 (1994).
13. Blow, J.J. Control of chromosomal DNA replication in the early *Xenopus* embryo. *EMBO J.* **20**, 3293–3297 (2001).
14. Lebofsky, R., Takahashi, T. & Walter, J.C. DNA replication in nucleus-free *Xenopus* egg extracts. *Methods Mol. Biol.* **521**, 229–252 (2009).
15. Yardimci, H., Loveland, A.B., Habuchi, S., van Oijen, A.M. & Walter, J.C. Uncoupling of sister replisomes during eukaryotic DNA replication. *Mol. Cell* **40**, 834–840 (2010).
16. Gary, R., Kim, K., Cornelius, H.L., Park, M.S. & Matsumoto, Y. Proliferating cell nuclear antigen facilitates excision in long-patch base excision repair. *J. Biol. Chem.* **274**, 4354–4363 (1999).
17. Harrington, J.J. & Lieber, M.R. The characterization of a mammalian DNA structure-specific endonuclease. *EMBO J.* **13**, 1235–1246 (1994).
18. Shen, B., Nolan, J.P., Sklar, L.A. & Park, M.S. Functional analysis of point mutations in human flap endonuclease-1 active site. *Nucleic Acids Res.* **25**, 3332–3338 (1997).
19. Blow, J.J. & Laskey, R.A. Initiation of DNA replication in nuclei and purified DNA by a cell-free extract of *Xenopus* eggs. *Cell* **47**, 577–587 (1986).
20. Walter, J. & Newport, J.W. Regulation of replicon size in *Xenopus* egg extracts. *Science* **275**, 993–995 (1997).
21. Herrick, J., Stanislawski, P., Hyrien, O. & Bensimon, A. Replication fork density increases during DNA synthesis in *X. laevis* egg extracts. *J. Mol. Biol.* **300**, 1133–1142 (2000).
22. Lucas, I., Chevrier-Miller, M., Sogo, J.M. & Hyrien, O. Mechanisms ensuring rapid and complete DNA replication despite random initiation in *Xenopus* early embryos. *J. Mol. Biol.* **296**, 769–786 (2000).
23. Blow, J.J., Gillespie, P.J., Francis, D. & Jackson, D.A. Replication origins in *Xenopus* egg extract are 5–15 kb apart and are activated in clusters that fire at different times. *J. Cell Biol.* **152**, 15–26 (2001).
24. Marheineke, K. & Hyrien, O. Control of replication origin density and firing time in *Xenopus* egg extracts. *J. Biol. Chem.* **279**, 28071–28081 (2004).
25. Marheineke, K. & Hyrien, O. Aphidicolin triggers a block to replication origin firing in *Xenopus* egg extracts. *J. Biol. Chem.* **276**, 17092–17100 (2001).
26. Ridelis, I. *et al.* Use of Kikume green-red fusions to study the influence of pharmacological chaperones on trafficking of G protein–coupled receptors. *FEBS Lett.* **586**, 784–791 (2012).
27. Herrick, J., Jun, S., Bechhoefer, J. & Bensimon, A. Kinetic model of DNA replication in eukaryotic organisms. *J. Mol. Biol.* **320**, 741–750 (2002).
28. Ayyagari, R., Gomes, X.V., Gordenin, D.A. & Burgers, P.M.J. Okazaki fragment maturation in yeast. I. Distribution of functions between FEN1 and DNA2. *J. Biol. Chem.* **278**, 1618–1625 (2003).
29. Hoskins, A.A., Gelles, J. & Moore, M.J. New insights into the spliceosome by single molecule fluorescence microscopy. *Curr. Opin. Chem. Biol.* **15**, 864–870 (2011).
30. Jain, A. *et al.* Probing cellular protein complexes using single-molecule pull-down. *Nature* **473**, 484–488 (2011).
31. Thompson, M.A., Biteen, J.S., Lord, S.J., Conley, N.R. & Moerner, W.E. Molecules and methods for super-resolution imaging. in *Single Molecule Tools, Part B: Super-Resolution, Particle Tracking, Multiparameter, and Force Based Methods* (ed. Walter, N.G.) Ch. 2, 27–59 (Academic Press, 2010).
32. Lord, S.J. *et al.* Azido push-pull fluorogens photoactivate to produce bright fluorescent labels. *J. Phys. Chem. B* **114**, 14157–14167 (2010).
33. Bates, M., Blosser, T.R. & Zhuang, X. Short-range spectroscopic ruler based on a single-molecule optical switch. *Phys. Rev. Lett.* **94**, 108101 (2005).
34. Conley, N.R., Biteen, J.S. & Moerner, W.E. Cy3-Cy5 covalent heterodimers for single-molecule photoswitching. *J. Phys. Chem. B* **112**, 11878–11880 (2008).
35. Patterson, G., Davidson, M., Manley, S. & Lippincott-Schwartz, J. Superresolution imaging using single-molecule localization. *Annu. Rev. Phys. Chem.* **61**, 345–367 (2010).

ONLINE METHODS

Microscope. Flow cells were mounted on an inverted microscope (IX-71, Olympus) and fluorescence was excited with objective-type TIR illumination through a high-NA objective (PLAPON 60× OTIRMF, NA 1.45, Olympus)[7,15]. For PhADE imaging of mKikR, a multiline argon-krypton laser (I-70 Spectrum, Coherent) provided the 568-nm excitation line, whereas the photoactivation line was from a diode-pumped, 405-nm laser (maximal output 50 mW, CrystaLaser). After magnification and filtering, the 568-nm and 405-nm lines were merged via a dichroic mirror (z405bcm, Chroma), and collimated light was focused on the back aperture of the objective with a converging lens (Thor Labs). TIR excitation with 405-nm and 568-nm lines was aligned empirically by offsetting the back focal lens during imaging of an aqueous solution of 100 nM rhodamine 110 and sulforhodamine 101. Fluorescence was collected through the same objective and passed through a dichroic mirror (T585lp, Chroma) and emission filter (ET620/60, Chroma) before 1.6× magnification onto an EM-CCD (iXon, Andor). The pixel size in sample space was 166 nm × 166 nm. Pulses of excitation and activation light were shutter-controlled (Uniblitz) by home-built code (LabView)[36]. The 488-nm line from the argon- krypton laser was used to image fluorescein and mKikG, and the 647-nm line was used to image Alexa Fluor 647 through standard FITC and Cy5 filter sets (Chroma). SYTOX Orange was excited with 568-nm light and imaged through the mKikR filter set.

Cloning, site-directed mutagenesis and protein expression. Recombinant *X. laevis* Fen1^{KikGR} was cloned in two steps. First, the mKikGR open reading frame (ORF) was amplified from pRSETb-6×His-mKikGR[7] using primers A and B (**Supplementary Table 3**) (IDT DNA) with flanking restriction sites, and the double digest was cloned into pET28b between the BamHI and XhoI sites. The ORF of the resulting plasmid pET28b-mKikGR-6×His was verified by sequencing. Second, *X. laevis fen1a* (*xfen1*) was amplified from pET28 2×FLAG-Fen1-GST-His[37] using primers C and D with flanking restriction sites, and the double digest was cloned into pET28b-mKikGR-6×His between the NcoI and NheI sites. *X. laevis* has a pseudo-tetraploid genome and, thus, two nonallelic genes *xfen1a* and *xfen1b* that differ by 4.5% of their amino acids[38]. Bibikova *et al.*[38] have shown that both protein products are active but that xFen1a is more abundantly expressed in oocytes. The ORF of the resulting plasmid pET28b-xFen1-mKikGR-6×His was verified by sequencing. Point mutants of Fen1^{KikGR} were made in plasmid pET28b-xFen1-mKikGR-6×His using the QuikChange Site-Directed Mutagenesis Kit (Stratagene) and the primers described in **Supplementary Table 3** (Operon and IDT DNA); the full ORFs were subsequently sequenced.

Fen1^{KikGR} was overexpressed and purified via Ni-NTA affinity with some modifications from the previously published protocol[37]. The expression plasmids were transformed in BL21(DE3) cells and selected with 50 μg ml^{-1} kanamycin. A volume of 0.5 l of cells was grown at 37 °C in LB medium with 50 μg ml^{-1} kanamycin to OD600, whereupon the temperature was turned down to 19 °C and overexpression was induced with 1 mM IPTG. From this step onward, care was taken to protect cells or protein-containing fractions from prolonged exposure to room light to limit premature photoconversion of the KikGR fluorophore. After 6 h of growth, cells were harvested by centrifugation, frozen in liquid nitrogen, and stored at −80 °C. For purification, the cells were thawed in Buffer A (20 mM HEPES, pH 8; 500 mM NaCl; 10% glycerol; 2 mM βME; 0.1% Igepal CA-630; 1 mM PMSF and 1 mM benzamidine) supplemented with cOmplete, EDTA-free Protease Inhibitor Cocktail Tablets (Roche) and 1 mg ml^{-1} lysozyme, and the cells were then lysed by sonication. All further steps were carried out at 4 °C. The lysates were cleared at 14,000 r.p.m. in an SS-34 rotor (Sorvall) for 30 min, supplemented with 7.5 mM imidazole pH 8 and incubated in batch with 1 ml of Ni-NTA (Qiagen) for 1 h. The Ni-NTA beads were washed in batch twice for 5 min with 25 bed volumes of Buffer A + 20 mM imidazole, pH 8. The beads were then loaded onto a column and washed with ten additional bed volumes of Buffer A + 20 mM imidazole, pH 8. Finally, the protein was eluted with 1.5 bed volumes of Buffer A + 250 mM imidazole, pH 8. Concentrated fractions, distinguishable by the green color of mKikGR, were pooled and dialyzed into storage buffer (50 mM Tris, pH 8; 300 mM NaCl; 1 mM EDTA; 1 mM DTT and 10% glycerol) and stored at −80 °C. Protein concentration was assessed by gel densitometry and Bradford assay with a BSA standard (Bio-Rad). These concentration measurements were compared to and found to agree with the concentration determined from the extinction coefficient for the 505-nm absorbance peak of the mKikG fluorophore. The photoactivation of KikG to KikR involves a beta elimination reaction that fragments the peptide backbone, allowing the extent of photoactivation to be monitored via SDS-PAGE[7]. Thus, the fraction of the Fen1^{KikGR} that could be photoconverted was determined by exposing a 0.1 mg ml^{-1} solution of the fusion protein to 405-nm light (0.01 W/cm^2) in a quartz cuvette for up to 1 h. Aliquots were taken at various time points, were separated by SDS-PAGE and stained with Coomassie, and the ratio of fragmented versus full-length Fen1^{KikGR} was determined by band densitometry. We found that 80% of wild-type Fen1^{KikG} could be converted to Fen1^{KikR} (**Supplementary Fig. 2c**).

Purification and characterization of p27^{Kip}, geminin and 6×His-mKikGR were previously described[7,39,40]. 6×His-mKikGR was biotinylated with EZ-link NHS-PEG$_4$-biotin per the manufacturer's instructions (Thermo Scientific).

Flow cell, DNA templates and surface tethering. Streptavidin-coated and PEG-passivated flow cells were assembled as detailed in ref. 41, except that (i) inlet tubing was limited to 5 cm in length (flow-cell volume including inlet tubing was ~6 μl) and (ii) ELB++ (10 mM HEPES-KCl, pH 7.7; 100 mM KCl; 2.5 mM $MgCl_2$ and 1 mg ml^{-1} BSA Fraction V (OmniPur, EMD)) was used to block non-specific binding to the glass and to flow in DNA. Two DNA templates were used. Biotin-λ-biotin DNA was prepared by ligating 12-mer oligonucleotides modified with 3′ biotin-TEG (IDT) (BL1 and BL2; **Supplementary Table 3**) to the complementary, single-stranded ends of λ DNA (N6-methyladenine free) (NEB)[41]. Biotin-λ-fill was prepared similarly, except BL2 was replaced with a nonbiotinylated oligo, L2 (**Supplementary Table 3**). A 30 pM solution of either DNA in ELB++ was drawn into the flow cell at 50 μl min^{-1} for 15 min to assemble double or single tethers, respectively. In real-time imaging experiments, biotinylated QDot605 (Invitrogen) were sparsely immobilized on the surface for use as fiducial markers. In either case, the flow cell was washed extensively (100 flow-cell volumes) with a replication-compatible buffer, ELB++, before extracts were added to start licensing and replication.

Single-molecule replication reactions. High-speed supernatant (HSS) extract and nucleoplasmic extract (NPE) were prepared from unfertilized *X. laevis* eggs as described previously[11,14]. After DNA substrates were assembled and washed, the DNA was licensed in HSS. HSS was supplemented with an ATP regeneration system (2 mM ATP, 20 mM phosphocreatine and 5 μg ml^{-1} creatine kinase), 15 μg ml^{-1} nocodazole and, to rescue licensing of the low concentration of λ DNA[15,42], 30 ng μl^{-1} of a DNA oligo duplex (same as QuikChange oligo pair for D179A (**Supplementary Table 3**) annealed in 10 mM Tris-HCl, pH 7.5; 50 mM NaCl and 0.1 mM EDTA by slow cooling from 95 °C to room temperature for 1 h). This oligo duplex was too short to be licensed itself[43]. Then, 20 μl of supplemented HSS was drawn into the flow cell at 10 μl min^{-1} for 2 min, flow was stopped and the reaction was allowed to proceed for 20 min at 22 °C.

Next, to promote efficient initiation and elongation only on the licensed λ DNA, a 'replication mix' of HSS and NPE containing nonreplicating carrier plasmid[42] was introduced into the flow cell. First, HSS was supplemented with the ATP regeneration system and nocodazole as describe above and 400 nM geminin. After 5 min at room temperature, carrier plasmid (pBS(−)KS II) was added at a final concentration of 15 ng μl^{-1}. Meanwhile, NPE was diluted to either 25% or 50% with buffer supplemented with the ATP regeneration system, 6.7 μM digoxigenin-dUTP (dig-dUTP) (Roche) and, if used, the appropriate concentration of Fen1^{KikGR}. Finally, after 5 min at 22 °C, 2 volumes of the NPE reaction were mixed with 1 volume of HSS supplemented with geminin and pBS(−)KS II (nonlicensed carrier plasmid). Of this replication mix, 15–30 μl was drawn into the flow cell at 10 μl min^{-1} to start replication.

To limit initiation on licensed λ DNA, the replication mix was drawn in for only 30–90 s and immediately replaced by, flowing at 10 μl min^{-1} for 1 min, the same mix supplemented with the Cdk inhibitor p27^{Kip} at 70 ng μl^{-1} as described previously[15].

α-Dig staining and measurement of replication bubbles. For studying replication on doubly tethered λ DNA, extracts but not all proteins bound to DNA were removed by flushing the flow cell with ELB++ for a total of 10 min at 10 μl min^{-1}. Under these conditions, singly tethered DNA remained compacted, whereas doubly tethered DNA remained extended. Next, dig-dUTP incorporation on doubly tethered λ DNA was stained with anti–digoxigenin-fluorescein Fab fragments (α-Dig) (Roche) and costained with SYTOX Orange (Invitrogen). Doubly tethered DNA was imaged in the absence of flow, α-Dig was excited with 488-nm light (2.3 W cm^{-2}, 100 ms) and SYTOX Orange was excited with 568-nm light (3.5 W cm^{-2}, 100 ms).

Replication bubbles were scored in custom MATLAB code. The SYTOX image was used to verify continuity and extension (minimum extension analyzed was 70% of contour length) of DNA. Profiles through the α-Dig signals were analyzed for replication bubbles. Stretches that were 2 pixels long and had a signal 50% above background were scored as the smallest bubbles. α-Dig stretches of >5 pixels were scored as two bubbles if a valley had less than half of the peak signal on either side. The length measurements were assumed to have an uncertainty of ±1 pixels or ±166 nm. This uncertainty was assumed to be independent and random. Error bars (error estimate) are the sum of the propagated error and the s.e.m.

Tracking bubble growth. For D179A Fen1^{KikR}-labeled replication bubbles that eventually reached a length-to-width ratio of at least 3:1 (suggesting they were on doubly tethered DNA), tracking began when the signal reached a threshold value, 2–4 times above background, and ended at 25 min or when the DNA compacted. Home-built MATLAB code measured the length of the signal above threshold over time and to the nearest pixel. Bubble length in pixels was converted to base pairs by multiplying by a stretching factor 48,502 bp per 80 pixels.

Scoring dynamics initiations. Origins were scored in custom MATLAB code on λ-DNA molecules that showed an end-to-end distance between D179A Fen1^{KikR} signals that was 70% to 90% of λ-DNA contour length, did not interact or shift, and were well illuminated. Such molecules were analyzed for up to 10 min after NPE addition or until the DNA tether compacted. Kymographs were inspected at multiple thresholds, and initiation events were scored that fulfilled the following criteria: the new D179A Fen1^{KikR} signal (i) was 50% above background, (ii) grew in intensity or size and (iii) did not disappear for more than one frame. (iv) If the D179A Fen1^{KikR} tract grew by more than 3 pixels (498 nm, ~1,800 bp) within 1 min (or three times the measured rate of bubble growth), a new initiation was scored in its middle. The latter criterion distinguished some origins firing close together such that their diffraction-limited images overlapped.

Concentration of D179A Fen1^{KikGR} needed to label replication bubbles. High concentrations of D179A Fen1^{KikGR} were used to label replication bubbles for real-time imaging. We noticed that the pattern of D179A Fen1^{KikGR} binding to λ DNA was concentration and extract dependent. For one pair of extracts, 4 μM D179A Fen1^{KikGR} led to stable binding of D179A Fen1^{KikR} along the entire length of the replication bubble as long as 15–20 min after NPE addition (**Fig. 2c**,**d** and **Supplementary Figs. 4b**,**e** and **5c**,**d**,). When three different pairs of HSS and NPE were used, addition of 2 μM D179A Fen1^{KikGR} was sufficient to achieve the same effect (**Figs. 2e**, **3** and **4b**–**g** and **Supplementary Figs. 3a**,**c**; **4c**,**d**,**f**,**g**; **5a**; **6** and **8**).

Imaging single molecules of Fen1^{KikR} on DNA. λ DNA was replicated in the presence of 125 nM or 250 nM Fen1^{KikGR} and imaged as described. Afterward, biotin-mKikGR was introduced to bind the surface at low densities, and single molecules were imaged as during replication. DNA was stained with α-Dig and SYTOX. Fen1^{KikR} and biotin-mKikR images were processed in ImageJ to flatten the illumination and subtract the background (using the Rolling Ball plug-in)[44]. In MATLAB, the Fen1^{KikR} molecules colocalizing with α-Dig tracts were chosen, and their integrated intensity within a 4 × 4–pixel region of interest (ROI) was measured over time. Events with intensities above a threshold were called 'on' after comparing similarly imaged and analyzed biotin-mKikR molecules. The number of ROIs that contained a signal was reported as 'Fen1 foci' (**Fig. 4b**,**c** and **Supplementary Fig. 6b**). For **Figure 4d**,**e** and **Supplementary Figure 7b**, ROIs with 'on' events in the first frame were isolated, and the number of consecutive 'on' frames was measured (for example, on time = 0 if the ROI was only 'on' in the first frame) and then compared to the on time for biotin-mKikGR.

doi:10.1038/nmeth.2174

Measuring the off rate of Fen1^{KikGR} from replication bubbles. During replication in the presence of 2 μM WT Fen1^{KikGR}, Fen1^{KikR} was activated and imaged. Extracts were removed; 1 ng ml^{-1} biotin-mKikGR was introduced into the flow cell to densely coat the streptavidin-coated surface; and, after extensive washing, biotin-mKikR was activated once and then imaged with 100-ms exposure of 568-nm light (3.5 W cm^{-2}) at 1 Hz for 50 frames to obtain the rate of photobleaching. The signal loss of Fen1^{KikR} from DNA was then compared to the photobleaching of surface-immobilized biotin-mKikR. First, the biotin-mKikR intensity in the region of interest defined by the DNA was integrated for each frame and the background value from the preactivation frame was subtracted. After normalization to the first-frame intensity, the vector was plotted against 568-nm exposure time and was well fit by a biexponential decay

$$y = A_1 e^{\frac{-x}{t_1}} + A_2 e^{\frac{-x}{t_2}} \quad (1)$$

where y is the normalized intensity, x is the exposure time, A_1 and A_2 are weighting coefficients for the decays and t_1 and t_2 are the mean lifetimes of the rapid blinking and slower bleaching decay routes. Similarly, the intensity of Fen1^{KikR} on DNA in the same ROI was integrated over time, a local background was subtracted and the intensity was normalized to the first frame. Because the majority of mKikR photodarkening during the imaging period was due to the fast blinking decay, we also fit the Fen1^{KikR} decay curves to a biexponential decay (equation (1)), where t_1 was fixed as the blinking mean lifetime measured from the biotin-mKikR bleaching curve and t_2 yielded the mean lifetime of Fen1^{KikR} on DNA.

36. Loparo, J.J., Kulczyk, A.W., Richardson, C.C. & van Oijen, A.M. Simultaneous single-molecule measurements of phage T7 replisome composition and function reveal the mechanism of polymerase exchange. *Proc. Natl. Acad. Sci. USA* **108**, 3584–3589 (2011).
37. Havens, C.G. & Walter, J.C. Docking of a specialized PIP box onto chromatin-bound PCNA creates a degron for the ubiquitin ligase CRL4Cdt2. *Mol. Cell* **35**, 93–104 (2009).
38. Bibikova, M. *et al.* Characterization of FEN-1 from *Xenopus laevis*. *J. Biol. Chem.* **273**, 34222–34229 (1998).
39. Walter, J.C. Evidence for sequential action of cdc7 and cdk2 protein kinases during initiation of DNA replication in *Xenopus* egg extracts. *J. Biol. Chem.* **275**, 39773–39778 (2000).
40. Wohlschlegel, J.A. *et al.* Inhibition of eukaryotic DNA replication by geminin binding to Cdt1. *Science* **290**, 2309–2312 (2000).
41. Yardimci, H., Loveland, A.B., van Oijen, A.M. & Walter, J.C. Single-molecule analysis of DNA replication in *Xenopus* egg extracts. *Methods*. published online, doi:10.1016/j.ymeth.2012.03.033 (6 April 2012).
42. Lebofsky, R., van Oijen, A.M. & Walter, J.C. DNA is a co-factor for its own replication in *Xenopus* egg extracts. *Nucleic Acids Res.* **39**, 545–555 (2011).
43. Edwards, M.C. *et al.* MCM2–7 complexes bind chromatin in a distributed pattern surrounding the origin recognition complex in *Xenopus* egg extracts. *J. Biol. Chem.* **277**, 33049–33057 (2002).
44. Abràmoff, M.D., Magalhães, P.J. & Ram, S.J. Image processing with ImageJ. *Biophotonics Int.* **11**, 36–42 (2004).